Nuclear Inst. and Methods in Physics Research, A 982 (2020) 164584

Contents lists available at ScienceDirect

Nuclear Inst. and Methods in Physics Research, A

journal homepage: www.elsevier.com/locate/nima

Super Spatial Resolution (SSR) method for small animal SPECT imaging: A Monte Carlo study

Roberto Massari [a], Annunziata D'Elia [a,b], Andea Soluri [c], Alessandro Soluri [a,*]

[a] Institute of Biochemistry and Cell Biology – National Research Council of Italy, Rome, Italy
[b] Department of Science, Section of Biomedical Sciences and Technologies, University "Roma Tre", Rome, Italy
[c] University "Tor Vergata", Rome, Italy

ARTICLE INFO

Keywords:
Small animal SPECT
Monte Carlo simulation
Super Spatial Resolution
Super resolution method

ABSTRACT

This work used Monte Carlo (MC) simulations in order to investigate the feasibility of the application of a super-resolution method, namely Super Spatial Resolution (SSR), to a preclinical SPECT system. The SSR method is used to obtain a resolution enhancement by combining several images containing slightly different perspectives of the same scene.

MC simulations are a useful tool in the development of new imaging devices, as well as in the assessment of new reconstruction methods. In this respect, GATE (Geant4 Application for Emission Tomography) is an open source platform dedicated to numerical MC simulations that has become a well validated toolkit for the simulation of SPECT and PET systems.

We modelled a four-headed preclinical SPECT scanner capable of the proper movements in order to obtain the SSR acquisition sequences. Each detector is based on a CsI(Tl) pixelated scintillator coupled to a low-energy tungsten collimator with parallel square holes.

Several phantoms and radioactive sources were simulated, in order to assess the performance of the proposed SPECT scanner. In addition, a complex voxelized phantom of a mouse was used to obtain realistic images with the aim of evaluating the system as a suitable tool for small animal imaging.

The whole system sensitivity was 164.1 cps/MBq. In order to assess the impact of the SSR this value must be divided by the number of the images acquired to perform this method. The average value of the trans-axial resolution improves from 2.4 mm to 1.54 mm, 1.21 mm and 1.03 mm by respectively applying the SSR based on two, three or four images. While the average axial resolution changes from 1.69 mm to 1.49 mm, 1.15 mm and 0.98 mm by respectively using the SSR based on two, three or four images. The mouse images obtained by using the voxel phantom have demonstrated the good capability of the system as a suitable tool for small animal imaging.

Finally, a comparison with commercial preclinical scanners has proved that the presented SSR scanner provides an alternative to pinhole SPECT systems for many preclinical research studies.

1. Introduction

Over the past decade, there has been a rapid rise in the use of small animal models in in-vivo biomedical research. As a consequence, small animal imaging has become an important tool in preclinical research, because the use of these techniques enables to investigate new drug molecules for disease diagnosis and therapy. This increasing interest was driven by the development of new multi-modality molecular imaging systems with improved performance. Indeed, a multi-modality system can effectively integrate functional morphological techniques.

Recently, new generation preclinical imaging systems have been introduced that combine traditional techniques like positron emission tomography (PET) or the single photon emission computed tomography (SPECT) and computed tomography (CT) or magnetic resonance imaging (MRI), with other imaging modalities such as optical and ultrasound [1]. In this context, the design of new devices must be addressed to improve their imaging performance. This can be accomplished through the introduction of innovative hardware systems and/or new software techniques.

Our group has developed in the past several high-performance scintigraphic detectors for small animal imaging [2,3]. Consequently, our interest is focused on developing small animal SPECT suitable for integration into multi-modality imaging systems.

* Correspondence to: Institute of Biochemistry and Cell Biology – National Research Council of Italy, c/o International Campus "A. Buzzati-Traverso", Via E. Ramarini, 32, 00015 Monterotondo Scalo (Roma), Italy.
E-mail address: alessandro.soluri@cnr.it (A. Soluri).

https://doi.org/10.1016/j.nima.2020.164584
Received 13 July 2020; Received in revised form 18 August 2020; Accepted 24 August 2020
Available online 25 August 2020
0168-9002/

In small animal SPECT imaging, the spatial resolution is an important parameter that influences the design of the scanner, since it is directly related to the small size of the organs. In particular, mice's organs are a thousand time smaller than the equivalent organs of humans, consequently preclinical scanner must exhibit spatial resolutions that are roughly ten times better than the clinical ones [4]. Clinical gamma cameras feature a spatial resolution of about one centimetre in working conditions, using parallel hole collimation [5]. Therefore, for small animal imaging a spatial resolution of millimetre or sub-millimetre is needed. However, this resolution improvement is achieved at the cost of a reduction in sensitivity of the SPECT system. Consequently, in the SPECT scanner design there is an inevitable trade-off between the detection efficiency and the spatial resolution [6].

As a general rule, the overall resolution of a scintigraphic system depends on the combined effect of the intrinsic detector resolution and the collimator resolution. Regarding the latter, there are several collimator designs that provide different behaviours.

While the parallel hole collimator is the most used in the clinical practice, pinhole or multi-pinhole collimators are commonly used for preclinical SPECT [7,8]. Under certain conditions, the use of pinhole collimators provides better spatial resolution and geometric efficiency with respect to the parallel hole collimation. Indeed, by using the parallel hole collimator the overall spatial resolution cannot be better than the intrinsic spatial resolution of the detector. Instead, by using the magnification of the image, due to the pinhole geometry, the observed spatial resolution can overcome this limitation. The spatial resolution and sensitivity of the system improve by placing the object closer to the pinhole aperture, but at the expense of a reduced field-of-view (FOV). It must be underlined that the pinhole collimator exhibits a rapid decrease in detection efficiency as the source-to-collimator distance increases, whereas for the parallel-hole collimators, within a certain degree, the efficiency remains constant. Although pinhole or multi-pinhole collimators provide better spatial resolution and sensitivity, because of the FOV limitation, the inhomogeneity of the spatial resolution and the axial blurring effect [5,9] the parallel hole collimation will be the most suitable option for whole body rodent imaging with good sensitivity [10,11].

Over the past few years, some groups have developed new detectors suitable for molecular imaging based on parallel hole collimators [12–15]. These solutions involve improvements of the intrinsic spatial resolution achieved through hardware enhancements. In this regard, in some of our previous works we presented the development of high-performance imaging detectors. Specifically, the described solutions involve improvements through the use of new scintillation materials [16], the use of new position sensitive photomultiplier Tubes (PSPMTs) [16] or silicon photomultipliers (SiPMs) [17], and the design of novel electronic readouts [18].

In order to design high resolution devices, a widely used choice is to employ pixelated scintillators, with the aim of minimizing the spread of scintillation light. Consequently, the achievable intrinsic spatial resolution is set by the pixel size [19]. However, a serious limitation with this point, is that scintillator pixelation techniques require a great deal of work and may be cost-prohibitive, especially for sub-millimetre pixels [20]. Furthermore, by reducing the scintillation element size several characteristics get worse: the detection efficiency drops due to the active-to-total volume ratio decreasing. This leads to the degradation of the output light which causes an increase in the pixel surface-to-volume ratio and the probability of absorption of the scintillation light increases too. Besides, inter-crystal Compton scattering events also increase.

In this respect, within the past decade, SiPMs have become an important component as an alternative to the more conventional PSPMTs. Indeed, these photodetectors have a gain similar to that of PSPMTs, fast timing properties, and they are insensitive to magnetic fields, which makes them a viable option to make systems MRI compatible [21,22]. However, the most interesting aspect is that the use of array of small SiPMs (e.g. size of 1 mm × 1 mm) provides a better sampling of the scintillation light distribution (SLD), thus improving the pixel identification. This makes it easier to effectively obtain detectors with sub-millimetre pixels.

As stated above, the overall resolution also depends on the collimator. Therefore, the next step consists in using a high-resolution collimator, but at the cost of its geometric efficiency of detection. Anyway, considering this, it can be imagined that below a certain pixel size the detector becomes difficult to implement.

In order to improve the detectability of the scintillation elements, our group has introduced a scintillation assembly made up of crystals integrated into a square hole tungsten structure. In particular, the use of tungsten septa between the crystals has the ability to reduce the inter-crystal Compton scatter and eliminates the optical crosstalk. As a result, the final image has a better contrast [23,24]. However, this solution becomes increasingly difficult to implement as the pixel size decreases. Moreover, we adopted a square hole collimator, for the imaging detectors we developed, in order to ensure the complete match between collimator holes and scintillation crystals. This alignment provides a better detection efficiency as compared with the use of a hexagonal hole collimator [17,25]. Furthermore, a better signal-to-noise ratio can be obtained through this solution due to the suppression of the mismatch between rectangular and hexagonal patterns [5].

The last years have been characterized by a huge growth in super-resolution techniques as an alternative to overcome the limits imposed by image sensors. The attractiveness of these methods lies in their capacity to produce an enhanced image combining a set of images provided by the detector.

The application of super-resolution techniques in clinical nuclear medicine equipment was investigated by our group, leading to the construction of a scintigraphic detector based on a proprietary patented method named Super Spatial Resolution (SSR) [26–28]. Previous works were only focused on the application of our method to two-dimensional images. The aim of this study is to evaluate the application of the SSR method to a SPECT imaging which is three-dimensional by definition. Here we present the performance assessment of our proposed super-resolution method through Monte Carlo (MC) simulations. In particular, we have studied the spatial resolution and system sensitivity of a preclinical SPECT system based on parallel-hole collimation.

2. Equipment and method

2.1. Super resolution algorithm

A super-resolution (SR) method is used to recover high-frequency details from several different images containing slightly different perspectives of the original scene. Typically, since this technique enables a resolution enhancement, the result image is called high-resolution (HR) image, while the input images are referred to as low-resolution (LR) images.

Various approaches have been proposed for solving the SR problem. Irani and Peleg in 1990 introduced an iterative back-projection (IBP) method working in the spatial domain [29]. The IBP algorithm estimates the HR image by back-projecting the error between simulated and measured LR images, thereby minimizing the error iteratively.

The collection of LR images must contain relative motion. SR reconstruction is only possible in coexistence with complementary spatial information which can be exploited to estimate the HR image. This is achievable through sub-pixel displacements obtained by an accurate movement of the imaging system.

In general, the displacements between LR images can be arbitrarily selected. However, the more different the LR images that are spaced in the sub-pixel range, the more non-redundant information they add to the HR reconstruction. This leads to the fact that evenly spaced displacements are ideal from an image reconstruction perspective, such that the LR images adequately sample the HR image [30]. Moreover, in order to make it easier to identify the spatial correspondence between

LR and HR pixels it is convenient to match the LR sampling points to the HR pixel grid.

Under these conditions, given a set of LR images each of $M \times N$ pixels, shifted by $1/m$ and $1/n$ of the LR pixel size along the horizontal and vertical direction respectively, the HR image will have a size of $mM \times nN$ pixels. Basically, the number of sub-pixel shifts becomes the magnification factor along a direction. For example, combining four $M \times N$ images acquired by moving the detector by half a pixel horizontally and vertically, we will obtain a $2M \times 2N$ image.

Typically, a preclinical SPECT system is made up of one or more detectors acquiring two-dimensional images mounted on a gantry that rotates around the small animal. Data acquisition depends on the way the gantry is moved. In the so-called step-and-shoot acquisition, the gantry stops at different angles for data acquisition, whereas, in the continuous acquisition, data are acquired as the gantry rotates. Then data are binned into discrete equivalent angular projections. The collected images provide the projection data needed for reconstructing the cross-sectional images (slices). Usually, for each slice, the two-dimensional image formed by the data collected over all of the projection angles is called sinogram. Finally, the stack of the contiguous slices, produced for all axial locations, forms the three-dimensional reconstructed volume.

The SR method as reported above is intended for two-dimensional images, and can be easily applied to each projection in the step-and-shoot acquisition. Indeed, the gantry can integrate a movement system able to provide the necessary sub-pixel displacements of the detectors. In this context, shifts on the axial direction provide an increase in the number of slices, while shifts on the tangential direction are able to increase the number of projection elements (bins) of the sinograms.

The overall scan time must be reasonably consistent with the animal's anaesthesia time, which can be estimated in about 30 min [31]. Since the acquisition time is limited, the sub-pixel movements can be only carried out in the tangential or axial direction, according to the ongoing study, thereby limiting the number of required projections. For example, by opting to apply the displacements only on the tangential direction is possible an improvement in terms of trans-axial resolution, limiting the overall acquisition time, anyway. In the light of this, we can therefore distinguish an axial, trans-axial or full SSR. Moreover, for simplicity's sake, hereinafter we will indicate the number N of the LR images used in the SSR with the notation N-step, e.g. a 4-step trans-axial SSR designates the algorithm implementation based on four LR views shifted on the tangential direction.

Finally, the proposed SSR algorithm was implemented by using C++ under Ubuntu 18.04 operating system.

2.2. Monte Carlo simulations

MC simulations are widely considered as a useful tool in the development of new imaging devices, as well as in the assessment of new reconstruction methods. In this respect, GATE (Geant4 Application for Emission Tomography) is an open source platform developed by the OpenGATE collaboration and dedicated to numerical MC simulations in medical imaging [32,33].

In this work, all simulations were obtained by using GATE v.8.2 running on a Workstation with two Intel Xeon CPU E5 2630 processors (10 cores each) and 64 GB of RAM.

2.2.1. Geometry of the SPECT scanner

Our objective is to develop a new SPECT system devoted to molecular imaging. As mentioned above, we already developed in the past several revisions of a small animal SPECT named HiRIS (High-Resolution Imaging System) [2]. These detectors were based on a Position-Sensitive Photomultiplier Tube (PSPMT) coupled with a scintillator array combined with a square-hole tungsten collimator.

The SPECT scanner, modelled in this study, was made of four heads positioned on a rotating gantry with a distance of 60 mm between opposite pairs of detectors, as shown in Fig. 1(a). Both trans-axial and axial field of view (FOV) of the system are 53 mm.

The detector module sketched in Fig. 1(b) was designed according to the HiRIS structure. It was based on a 44 × 44 CsI(Tl) crystal array which provides a field of view (FOV) of 53 mm square. The crystal elements, each of size 1.0 mm × 1.0 mm × 5.0 mm, were optically isolated by using 200 μm of white epoxy reflector, thus obtaining a resulting pitch of 1.2 mm.

Each detector was equipped with a low energy parallel-square-hole collimator made up of tungsten. The 36 mm thick collimator was designed with a hole size of 1.0 mm and a septal thickness of 200 μm in order to ensure the perfect match between collimator channels and scintillation crystals and consequently improving the detector's performance [25].

Behind the scintillator, a 4.5 mm thick slab of polymethyl methacrylate (PMMA) models the back-compartment which contains the SiPMs and the readout electronics (e.g. S13361-2050NE-08 from Hamamatsu Photonics K.K. coupled to a charge division circuit). Finally, the whole detector is surrounded by a 2 mm thick lead shielding.

With regard to the SSR method, our scanner model manages to specify the lateral shift of the heads in the trans-axial plane and the axial shift during the tomographic scan in order to provide the proper acquisition sequence, as illustrated in Fig. 2. The detector shifts, in the lateral and axial direction, depend on the number of the LR images to acquire for SSR, as described in Section 2.1. Therefore, a 2-step SSR will require movements of a half a pixel in the selected direction (lateral and/or axial), i.e. 0.6 mm, for a 3-step SSR the shift must be 0.4 mm, and for a 4-step SSR the shift is 0.3 mm.

2.2.2. Digitizer chain

Interactions in which photons deposited energy within the scintillator crystals were considered to be detected events. The GATE *Digitizer* module simulates the behaviour of the detector's signal processing chain. The readout process was modelled by using an energy-centroid approach which is closer to the behaviour of a charge division circuit usually used as readout system. A Gaussian blur is applied to the energy deposited in order to represent the camera's energy resolution, with an average for each crystal of 15% referenced at 140.6 keV (gamma emission from ^{99m}Tc, commonly used in nuclear imaging).

Finally, given the relatively low energy of the gammas used for SPECT imaging, an energy window discriminator between 10 and 250 keV is applied via the *Thresholder* and *Upholder* modules.

2.2.3. Radioactive sources and phantoms

In order to assess the performance of the proposed SPECT system, several phantoms and radioactive sources were simulated.

Point source a point source, with a mono-energetic gamma emission of 140.6 keV and an activity of 3.7 MBq (0.1 mCi), was defined at the centre of the FOV.

Four-point sources phantom a set of four point sources was modelled at four different radial distances of 0, 10, 20 and 25 mm from the centre of the FOV and was repeated at four different axial positions of −25, -10, 10 and 25 mm with reference to the centre of the FOV. Each point source consists of a spherical source of 0.2 mm with a mono-energetic gamma emission of 140.6 keV. The total activity was 3.7 MBq (0.1 mCi).

Derenzo phantom: the phantom consists of a PMMA disc with a diameter of 30 mm and a thickness of 10 mm, which contains several water cylinders grouped in six sectors according to their diameter, as shown in Fig. 3. The diameters of the cylinders range from 0.8 to 1.8 mm, while their height is of 8 mm. Within each sector, the distance between the centres of two adjacent cylinders is the double of their diameter. A mono-energetic gamma emission of 140.6 keV was defined in correspondence to the volume of the cylinders, for a total activity of 37 MBq (1 mCi). The phantom was placed at the centre of the FOV aligned to the axial direction.

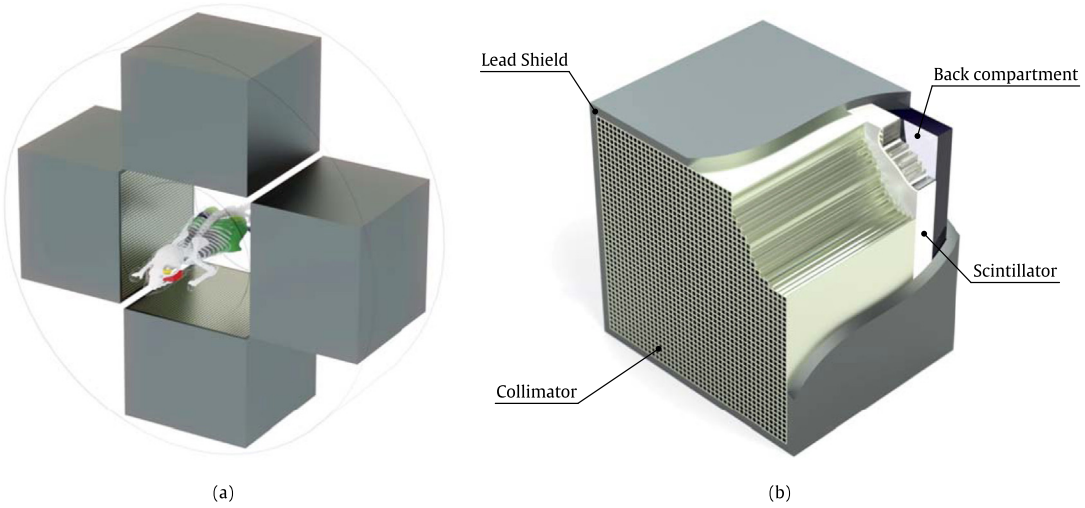

Fig. 1. Monte Carlo SPECT system model. From left to right: (a) SPECT scanner with Digimouse phantom, (b) Detector head structure.

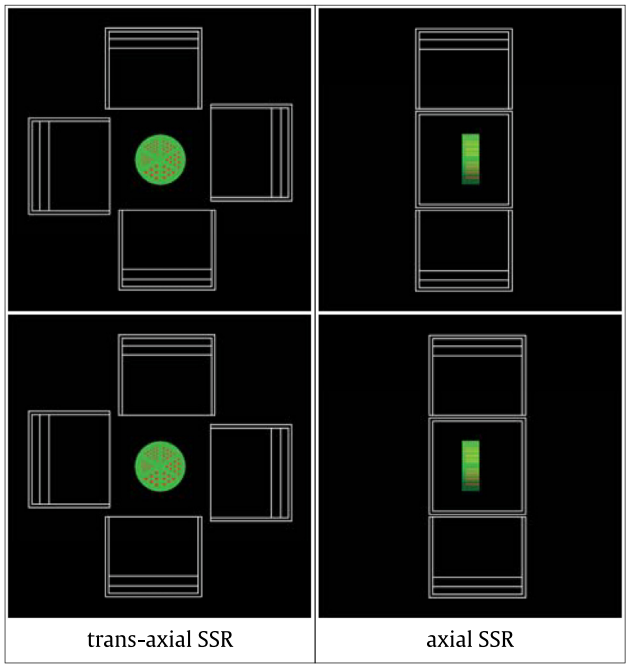

Fig. 2. Movements of the detectors for SSR acquisition (the displacements are magnified to make them evident).

Digimouse phantom: a three-dimensional volumetric phantom was used to obtain realistic images. This phantom was generated using co-registered CT and cryosection images of a nude normal male mouse [34]. The data consists in 380 × 992 × 208 matrix of 0.1 mm cubical voxels. From these data it was been defined an atlas of segmented organs and structures. In order to simulate realistic acquisitions, the CT scan was used to define the numerical phantom, by associating the appropriate material to each Hounsfield Unit (HU) value encoded in the CT data. In the meantime, the segmented atlas data was used to define the radioactive emission map by converting each voxel into an activity value by means of a proper translation table. Specifically, in order to simulate a bone scan, a mono-energetic gamma emission of 140.6 keV with an activity of 62.6 Bq/voxel was assigned to the voxels corresponding to the skeleton on the segmented atlas data, for a total activity of about 74 MBq (2 mCi). Furthermore, to assess the neurological imaging capabilities of the system an activity of 71.5 Bq/voxel was assigned to the volume of the corpus striatum, 14.3 Bq/voxel to the rest of the brain and the eyes, and 1.43 Bq/voxel was set to the other voxels of the body, for a total activity of about 37 MBq (1 mCi).

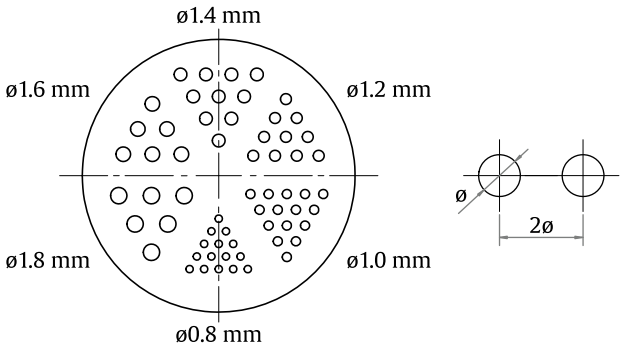

Fig. 3. Derenzo phantom.

2.2.4. Data output

SPECT imaging was obtained by collecting 64 projection views over 360° in step-and-shoot mode, which results in 16 acquisitions over an arc of 90° since the system is four-headed. For each view the proper shifts of the heads were applied, in order to obtain the SSR acquisition sequences.

The MC simulations results are stored in ROOT format files [35] for further analysis. This output files contain data about each single detection event in terms of particle type, kind of interaction, energy deposited, as well as spatial coordinates referred to the scanner geometry.

Simulations output data analysis was accomplished by using a C++ specifically developed software, which generates the single projection imaging for each detector head from the spatial position and energy of the individually detected gamma-rays, by using a 20% symmetric energy window for scatter rejection.

The SPECT images have been reconstructed by using the filtered back projection (FBP) algorithm in 2D projections of the STIR (Software for Tomographic Image Reconstruction) software [36], and analysed by using Mango image processing software [37].

2.3. Performance evaluation

With the aim of evaluating the behaviour and the performance of the system, several simulation set-ups were implemented.

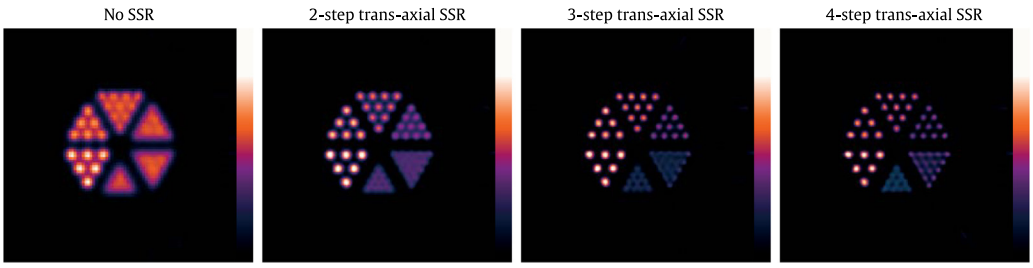

Fig. 4. Derenzo phantom. Trans-axial slice of the Derenzo phantom reconstructions, with and without SSR.

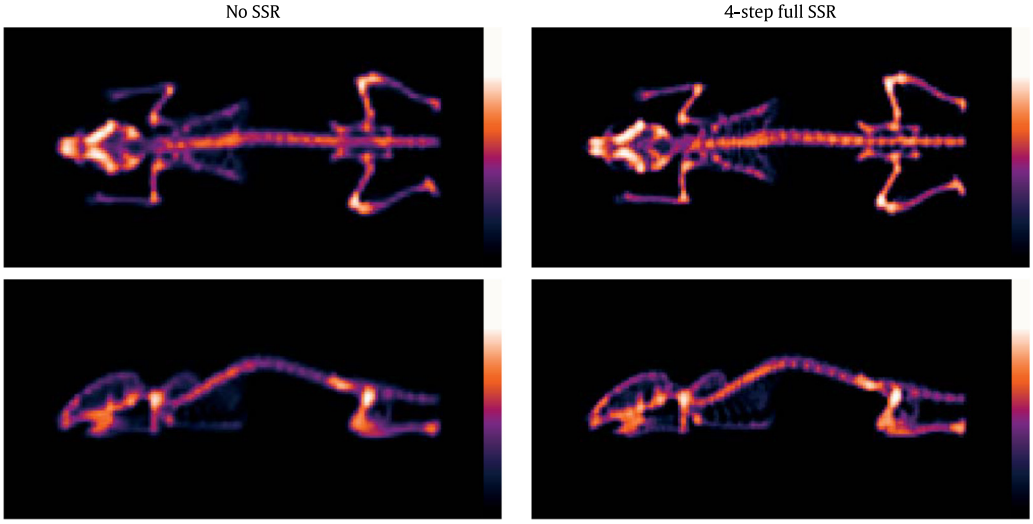

Fig. 5. Digimouse phantom bone scan simulation with and without SSR.

Table 1
Trans-axial SSR: spatial resolution in different radial offsets.

Radial offset (mm)	NO SSR		SSR 2		SSR 3		SSR 4	
	Tangential FWHM (mm)	Radial FWHM (mm)	Tangential FWHM (mm)	Radial FWHM (mm)	Tangential FWHM (mm)	Radial FWHM (mm)	Tangential FWHM (mm)	Radial FWHM (mm)
0	2.55	2.49	1.73	1.54	1.35	1.18	1.11	0.96
10	2.36	2.33	1.70	1.59	1.28	1.24	1.05	1.09
20	2.27	2.39	1.67	1.37	1.27	1.10	1.08	0.94
25	2.35	2.50	1.65	1.10	1.27	1.01	1.08	0.92

2.3.1. System sensitivity

The in-air system sensitivity was evaluated using the point source by calculating the collected counts over the acquisition time ratio. The sensitivity assessment was carried out within a 60 s data-acquisition period and by using a 20% symmetric energy window.

2.3.2. SPECT spatial resolution

The four-point sources phantom was utilized for the assessment of the SPECT spatial resolution which was measured in terms of full-width-at-half-maximum (FWHM) of the point spread function (PSF) obtained at the corresponding source's positions. In addition, in the trans-axial plane the spatial resolution was measured along the radial and tangential direction. The acquisition time for each projection step was 1 min.

2.3.3. Imaging performance

The Derenzo phantom was used to assess the overall imaging performance of the system. The time acquisition for each view of this phantom was 3 min.

Moreover, realistic-like scans were obtained by using the Digimouse phantom. In this case, the SPECT scan was obtained by setting a total acquisition time of 32 min coherently with the mouse's anaesthesia time.

Table 2
Axial SSR: spatial resolution in different radial offsets.

Radial offset (mm)	NO SSR FWHM (mm)	SSR 2 FWHM (mm)	SSR 3 FWHM (mm)	SSR 4 FWHM (mm)
0	1.56	1.37	1.02	0.87
10	1.64	1.49	1.10	0.94
20	1.76	1.53	1.22	1.03
25	1.81	1.56	1.25	1.06

3. Results and discussion

A dedicated small animal SPECT scanner was simulated by using the GATE MC platform, in order to assess the implementation of the SSR method applied to molecular imaging.

The estimate of the whole system sensitivity was 164.1 cps/MBq. It is reasonable to assess the impact of the SSR by dividing this value by the number N of the LR views exploited by the method.

The trans-axial resolution assessment for the trans-axial SSR in terms of FWHM along radial and tangential directions as functions of the radial position, are summarized in Table 1. The average value of the trans-axial resolution improves from 2.4 mm to 1.54 mm, 1.21 mm

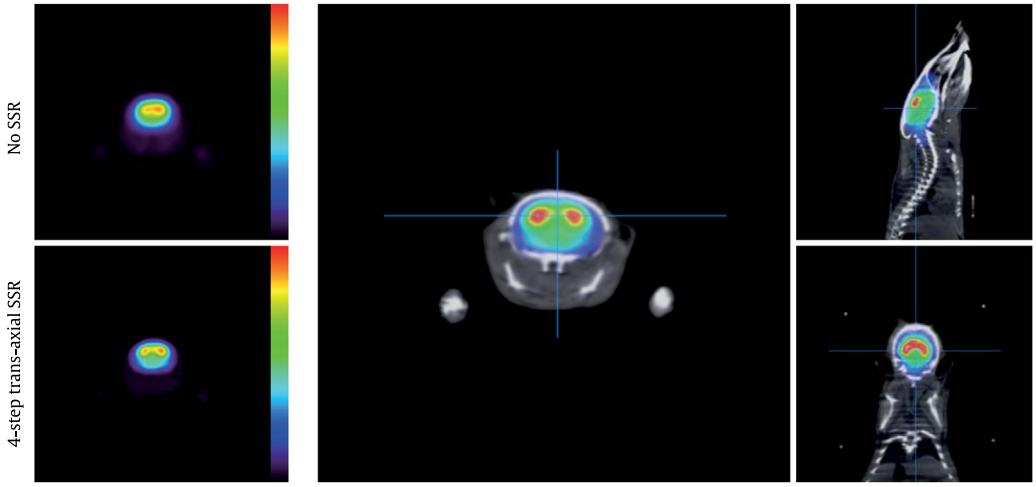

Fig. 6. Digimouse phantom neurological imaging simulation. Left: same slice of the SPECT reconstruction with and without SSR. Right: SPECT/CT fusion images obtained with 4-step trans-axial SSR.

and 1.03 mm by respectively applying the 2-step, 3-step and 4-step trans-axial SSR algorithm.

Table 2 reports the axial resolution values obtained by the axial SSR, the average value of the axial resolution changes from 1.69 mm to 1.49 mm, 1.15 mm and 0.98 mm by respectively using the 2-step, 3-step and 4-step axial SSR method.

Fig. 4 shows one trans-axial slice of the reconstructed image of the Derenzo phantom with and without trans-axial SSR enhancement.

Fig. 5 shows the Digimouse bone scan images obtained without and with the application of the 4-step full SSR method, in order to improve both the trans-axial and axial spatial resolution.

The simulated neurological imaging is illustrated in Fig. 6, where a comparison between the trans-axial images obtained without and with the 4-step trans-axial SSR method is displayed. The same figure shows the fused SPECT/CT images achieved by overlaying the SPECT image on top of the co-registered CT image that was already used to define the numerical phantom.

The results derived from simulations clearly demonstrate an improvement in terms of spatial resolution. Indeed, as illustrated in Fig. 4, the Derenzo phantom images become visually clearer as the number of LR images used in SSR increases. Finally, the image shows an adequate resolving in the section containing 1.0 mm rods for the 4-step SSR.

The system provides appropriate values of sensitivity and resolution which are suitable for preclinical applications. In Fig. 7 the proposed system is compared to several commercial preclinical SPECT scanners, Albira (Oncovision, Valencia, ES, EU), Inveon (Siemens Medical Solutions, Knoxville, TN, USA), U-SPECT-II (MILabs, Utrecht, NL, EU), NanoSPECT (BioScan, Washington DC, USA) and X-SPECT (Gamma Medica, Northridge, CA, USA) in terms of sensitivity and resolution values, on the basis of literature [38–40].

The mouse images obtained by using the Digimouse voxel phantom demonstrates the good capability of the system as a suitable tool for small animal imaging. In the simulated bone scan, the skeletal structures of the mouse are clearly imaged. Similarly, the imaging of small cerebral structures such as the corpus striatum provides an excellent map of regional cerebral function.

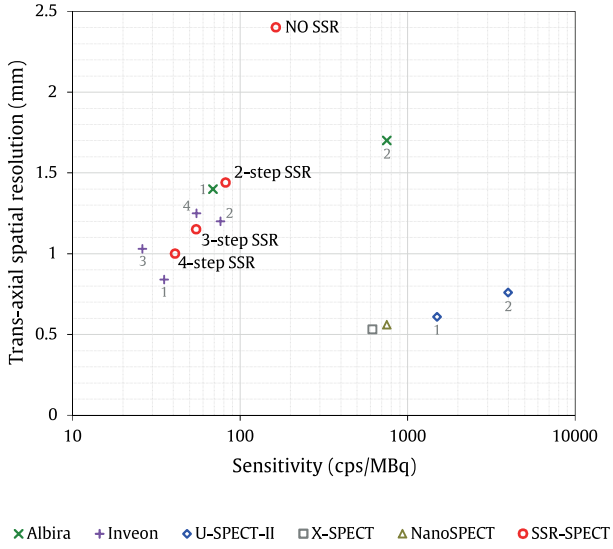

Fig. 7. Trans-axial spatial resolution as function of sensitivity. Albira: 1. single pinhole 1.0 mm trans-axial FOV 50 mm; 2. multi-pinhole 1.0 mm trans-axial FOV 50 mm. Inveon: 1. pinhole 0.5 mm, radius of rotation (ROR) 25 mm; 2. pinhole 1.0 mm, ROR 25 mm; 3. pinhole 0.5 mm, ROR 30 mm; 4. pinhole 1.0 mm, ROR 30 mm. U-SPECT-II: 1. multi-pinhole 0.6 mm, ROR 22 mm; 2. multi-pinhole 1.0 mm, ROR 22 mm. X-SPECT: multi-pinhole 1.0 mm, ROR 30 mm. NanoSPECT: multi-pinhole 1.0 mm, ROR 30 mm.

4. Conclusions

This paper describes the implementation of the SSR method applied to a preclinical SPECT system based on parallel-hole collimation.

In conclusion, the results derived from our simulations clearly demonstrate the feasibility of the SSR approach providing improved image quality. With the appropriate SSR configuration, a whole body millimetre spatial resolution can be achieved with a FOV suitable for mice and/or rats. Evidently, using a scanner design featuring a smaller pixel size a sub-millimetre resolution could be achievable, but at the cost of a reduction in sensitivity of the system.

In comparison with other commercial preclinical scanners, the system performance indicates that our solution may represents an alternative to pinhole SPECT systems for many preclinical research studies. In fact, multi-pinhole systems may exhibit better performance in terms of resolution and sensitivity, but the parallel-hole collimation offers advantages in terms of FOV and homogeneity of the spatial resolution and sensitivity. These are desirable features for quantitative imaging. Furthermore, an interesting aspect is that the SSR scan mode can be easily adapted according to the ongoing study, so as to optimize the system performance in terms of spatial resolution and sensitivity.

In our view, these results represent a preliminary step to the design process of a small animal SPECT suitable for integration into multi-modality imaging systems. We are currently developing innovative scintigraphic detectors based on SiPMs featuring a FOV of about 5 cm

× 10 cm. Future work will focus on the development of a preclinical SPECT based on this technology and integrating the SSR method.

CRediT authorship contribution statement

Roberto Massari: Conceptualization, Methodology, Software, Validation, Writing - original draft. **Annunziata D'Elia:** Data curation, Investigation, Writing - review & editing. **Andea Soluri:** Data curation, Voxel phantom setup. **Alessandro Soluri:** Methodology, Supervision.

Declaration of competing interest

The authors declare that they have no known competing financial interests or personal relationships that could have appeared to influence the work reported in this paper.

References

[1] R.Y. Lu, K. Yang, K. Zhou, B. Pang, G. Wang, Y. Ding, Q. Zhang, H. Han, J. Tian, C. Li, R. Q, An integrated quad-modality molecular imaging system for small animals, J. Nucl. Med. 55 (8) (2014) 1375.

[2] C. Trotta, R. Massari, G. Trinci, N. Palermo, S. Boccalini, F. Scopinaro, A. Soluri, High-resolution imaging system (HiRIS) based on H9500 PSPMT, Nucl. Instrum. Methods A 593 (2008) 454.

[3] R. Massari, A. D'Elia, A. Soluri, A new high-resolution imaging system (HiRIS2) detector for preclinical SPECT imaging, Nucl. Instrum. Methods A 917 (2019) 25.

[4] J. Mejia, M.A. Reis, A.C.C. Miranda, I.R. Batista, M.R.F. Barboza, M.C. Shih, G. Fu, C.T. Chen, L.J. Meng, R.A. Bressan, E.J. Amaro, Performance assessment of the single photon emission microscope: high spatial resolution SPECT imaging of small animal organs, Braz. J. Med. Biol. Res. 46 (11) (2013) 936.

[5] F. Scopinaro, R. Massari, A.D. Varvarigou, C. D'Alessandria, C. Trotta, G.P. Di Santo, A. Soluri, High resolution small animal single photon emission computed tomography: uptake of [99mTc]bombesin and [123I]ioflupane by rat brain, Q J Nucl. Med. Mol. Imaging 51 (2) (2007) 204.

[6] R.A. de Kemp, F.H. Epstein, C. Catana, B.M. Tsui, E.L. Ritman, Small-animal molecular imaging methods, J. Nucl. Med. 51 (5) (2010) 18S.

[7] T. Aoi, T. Zeniya, H. Watabe, H.M. Deloar, T. Matsuda, H. Iida, System design and development of a pinhole SPECT system for quantitative functional imaging of small animals, Ann. Nucl. Med. 20 (3) (2006) 245.

[8] L. Chen, B.M.W. Tsui, G.S.P. Mok, Design and evaluation of two multi-pinhole collimators for brain SPECT, Ann. Nucl. Med. 31 (8) (2017) 636.

[9] P.L. Krench, J. Lin, M.C. Gregoire, S.R. Meikle, An investigation of inconsistent projections and artefacts in miltipinhole SPECT with axially aligned pinholes, Phys. Med. Biol. 56 (23) (2011) 7487.

[10] Y. Qi, Optimized collimator designs for small animal SPECT imaging with a compact gamma camera, in: Conf Proc IEEE Eng Med Biol Soc., vol. 2005, 2005, pp. 1780.

[11] S.R. Meikle, P.L. Kench, J. Lin, Design considerations of small-animal SPECT cameras, in: Molecular Imaging of Small Animals, Springer-Verlag, New York, 2014, pp. 135–162.

[12] M. Georgiou, E. Fysikopoulos, K. Mikropoulos, E. Fragogeorgi, G. Loudos, Characterization of γ-Eye: a low-cost benchtop mousesized gamma camera for dynamic and static imaging, Mol. Imaging Biol. 19 (3) (2017) 398.

[13] S. Sajedi, N. Zeraatkar, V. Moji, M.H. Farahani, S. Sarkar, H. Arabi, B. Teymoorian, P. Ghafarian, A. Rahmim, M.R. Ay, Design and development of a high resolution animal SPECT scanner dedicated for rat and mouse imaging, Nucl. Instrum. Methods A 741 (2014) 169.

[14] Q. Zhang, S. Li, Z. Xie, Y. Lu, K. Yang, Q. Ren, Development of a small animal SPECT imager with LYSO scintillator arrays and PSPMTs, in: The 6th 2013 Biomedical Engineering International Conference, 2013, p. 1.

[15] H.C. Liang, M.L. Jan, J.L. Su, Development of a pixelated detector for clinical positron and single-photon molecular imaging, J. Med. Biol. Eng. 32 (5) (2011) 373.

[16] R. Massari, A. D'Elia, A. Soluri, Preliminary results on a small animal SPECT system based on H13700 PSMPT coupled with CRY018 array, Nucl. Instrum. Methods A 940 (2019) 296.

[17] R. Massari, A. Ucci, C. Campisi, F. Scopinaro, A. Soluri, A novel fully integrated handheld gamma camera, Nucl. Instrum. Methods A 832 (2016) 271.

[18] R. Massari, D. Caputo, S. Ronchi, A. Soluri, Low-power charge division circuits for wireless applications based on silicon photomultipliers, IEEE Sens. J. 16 (23) (2016) 8214.

[19] W.W. Moses, V. Gayshan, A. Gektin, The evolution of SPECT – from anger to today and beyond, in: Radiation Detectors for Medical Imaging, in: NATO Security Through Science Series, Springer, Dordrecht, The Netherlands, 2006, pp. 37–80.

[20] D. Uzun Ozsahin, L. Blckberg, G. El Fakhri, H. Sabet, GATE Simulation of a new design of pinhole SPECT system for small animal brain imaging, J. Instrum 12 (1) (2017) C01085.

[21] J.E. Mackewn, C.W. Lerche, B. Weissler, K. Sunassee, R.T.M. de Rosales, A. Phinikaridou, A. Salomon, R. Ayres, T. Charalampos, G.M. Soultanidis, P. Gebhardt, T. Schaeffter, P.K. Marsden, V. Schulz, PET performance evaluation of a pre-clinical SiPM-based MR-compatible PET scanner, IEEE Trans. Nucl. Sci. 62 (2015) 784.

[22] G. Llosá, C. Lacasta, N. Belcari, M.G. Bisogni, G. Collazuol, S. Marcatili, P. Barrillon, S. Bondil-Blin, C. de la Taille, C. Piemonte, A. Del Guerra, Monolithic 64-channel SiPM matrices for small animal PET, in: 2009 IEEE Nuclear Science Symposium Conference Record, 2009, pp. 1-5, 2658.

[23] Y. Shao, S.R. Cherry, S. Siegel, R.W. Silverman, A study of intercrystal scatter in small scintillator arrays designed for high resolution PET imaging, IEEE Trans. Nucl. Sci. 43 (3) (1996) 1938.

[24] C.S. Levin, M.P. Tornai, S.R. Cherry, L.R. MacDonald, E.J. Hoffman, Compton scatter and x-ray crosstalk and the use of very thin inter-crystal septa in high resolution PET detectors, in: Nuclear Science Symposium and Medical Imaging Conference Record (NSS/MIC), Vol. 2, IEEE, 1995, p. 1036.

[25] W. Chang, M. Rozler, S.D. Metzler, SPECT Instrumentation, in: Physics of PET and SPECT Imaging, CRC Press, Boca Raton, FL, USA, 2017, pp. 115–161.

[26] G. Trinci, R. Massari, M. Scandellari, F. Scopinaro, A. Soluri, Super spatial resolution (SSR) method for scintigraphic imaging, Nucl. Instrum Meth. A 626-627 (2011) 120.

[27] A. Soluri, G. Atzeni, A. Ucci, T. Bellone, F. Cusanno, G. Rodilossi, R. Massari, New device based on the super spatial resolution (SSR) method, Nucl. Instrum. Methods A 728 (2013) 150.

[28] A. Soluri, R. Massari, Patent Scintigraphic device with super spatial resolution, MI2008A1798 10/10/2008 – *U S* number 12/467, 566 18/05/2009, 2008.

[29] M. Irani, S. Peleg, Super resolution from image sequences, in: Proceedings. 10th International Conference on Pattern Recognition, vol. ii, 1990, p. 115.

[30] D. Robinson, P. Milanfar, Statistical performance analysis of superresolution, IEEE Trans. Image Process. 15 (2006) 1413.

[31] O. Ivashchenko, F. van der Have, M.C. Goorden, R.M. Ramakers, F.J. Beekman, Ultra-high-sensitivity submillimeter mouse SPECT, J. Nucl. Med. 56 (3) (2015) 470.

[32] G. Santin, D. Strul, D. Lazaro, L. Simon, M. Krieguer, M.V. Martins, V. Breton, C. Morel, GATE: a Geant4-based simulation platform for PET and SPECT integrating movement and time management, IEEE Trans. Nucl. Sci. 50 (5) (2003) 1516.

[33] S. Jan, G. Santin, D. Strul, S. Staelens, K. Assi'e, D. Autret, S. Avner, R. Barbier, M. Bardi'es, P.M. Bloomfield, D. Brasse, V. Breton, P. Bruyndonckx, I. Buvat, A.F. Chatziioannou, Y. Choi, Y.H. Chung, C. Comtat, D. Donnarieix, L. Ferrer, S.J. Glick, C.J. Groiselle, D. Guez, P.F. Honore, S. Kerhoas-Cavata, A.S. Kirov, V. Kohli, M. Koole, M. Krieguer, D.J. van der Laan, F. Lamare, G. Largeron, C. Lartizien, D. Lazaro, M.C. Maas, L. Maigne, F. Mayet, F. Melot, C. Merheb, E. Pennacchio, J. Perez, U. Pietrzyk, F.R. Rannou, M. Rey, D.R. Schaart, C.R. Schmidtlein, L. Simon, T.Y. Song, J.M. Vieira, D. Visvikis, R. Van de Walle, E. Wiers, C. Morel, GATE: a simulation toolkit for PET and SPECT, Phys. Med. Biol. 49 (19) (2004) 4543.

[34] B. Dogdas, A. Stout, A. Chatziioannou, R.M. Leahy, Digimouse: a 3d whole body mouse atlas from CT and cryosection data, Phys. Med. Biol. 52 (2007) 577.

[35] R. Brun, F. Rademakers, ROOT - An object oriented data analysis framework, Nucl. Instrum. Methods A 389 (1–2) (1997) 81.

[36] K. Thielemans, C. Tsoumpas, S. Mustafovic, T. Beisel, P. Aguiar, N. Dikaios, M.W. Jacobson, STIR: software for tomographic image reconstruction release 2, Phys. Med. Biol. 57 (4) (2012) 867.

[37] J.L. Lancaster, M. Martinez, Mango - Multi-image Analysis GUI, available at: http://www.ric.uthscsa.edu/mango (accessed on July 13th, 2020).

[38] T.J. Spinks, D. Karia, M.O. Leach, G. Flux, Quantitative PET and SPECT performance characteristics of the albira trimodal pre-clinical tomograph, Phys. Med. Biol. 59 (3) (2014) 715.

[39] S. Deleye, R. Van Holen, J. Verhaeghe, S. Vandenberghe, S. Stroobants, S. Staelens, Performance evaluation of small animal multipinhole spect scanners for mouse imaging, Eur. J. Nucl. Med. Mol. Imaging 40 (5) (2013) 744.

[40] K. Magota, N. Kubo, Y. Kuge, K.I. Nishijima, S. Zhao, N. Tamaki, Performance characterization of the inveon preclinical small-animal PET/SPECT/CT system for multimodality imaging, Eur. J. Nucl. Med. Mol. Imaging 38 (4) (2011) 742.